**Applied
Magnetic Resonance**

ORIGINAL PAPER

Advanced Magnetic Resonance Studies of Tetraphenyl-porphyrinatoiron(III) Halides

Pagnareach Tin, et al. *[full author details at the end of the article]*

Abstract

High-Frequency and -Field EPR (HFEPR) studies of Fe(TPP)X (X = F, Cl, Br; I, TPP^{2-} = *meso*-tetraphenylporphyrinate dianion) and far-IR magnetic spectroscopic (FIRMS) studies of Fe(TPP)Br and Fe(TPP)I have been conducted to probe magnetic intra- and inter-Kramers doublet transitions in these $S = 5/2$ metalloporphyrin complexes, yielding zero-field splitting (ZFS) and *g* parameters for the complexes: Fe(TPP)F, $D = +4.67(1)$ cm^{-1}, $E = 0.00(1)$ cm^{-1}, $g_\perp = 1.97(1)$, $g_\parallel = 2.000(5)$ by HFEPR; Fe(TPP)Cl, $D = +6.458(2)$ cm^{-1}, $E = +0.015(5)$ cm^{-1}, $E/D = 0.002$, $g_\perp = 2.004(3)$, $g_\parallel = 2.02(1)$ by HFEPR; Fe(TPP)Br, $D = +9.03(5)$ cm^{-1}, $E = +0.047(5)$ cm^{-1}, $E/D = 0.005$, $g_{iso} = 1.99(1)$ by HFEPR and $D = +9.05$ cm^{-1}, $g_{iso} = 2.0$ by FIRMS; Fe(TPP)I, $D = +13.84$ cm^{-1}, $E = +0.07$ cm^{-1}, $E/D = 0.005$, $g_{iso} = 2.0$ by HFEPR and $D = +13.95$ cm^{-1}, $g_{iso} = 2.0$ by FIRMS (the sign of E was in each case arbitrarily assigned as that of D). These results demonstrate the complementary nature of field- and frequency-domain magnetic resonance experiments in extracting with high accuracy and precision spin Hamiltonian parameters of metal complexes with $S > 1/2$. The spin Hamiltonian parameters obtained from these experiments have been compared with those obtained from other physical methods such as magnetic susceptibility, magnetic Mössbauer spectroscopy, inelastic neutron scattering (INS), and variable-temperature and -field magnetic circular dichroism (VT-VH MCD) experiments. INS, Mössbauer and MCD give good agreement with the results of HFEPR/FIRMS; the others not as much. The electronic structure of Fe(TPP)X (X = F, Cl, Br, I) was studied earlier by multi-reference *ab initio* methods to explore the origin of the large and positive *D*-values, reproducing the trends of *D* from the experiments. In the current work, a simpler model based on Ligand Field Theory (LFT) is used to explain qualitatively the trend of increasing ZFS from X = F to Cl to Br and to I as the axial ligand. Tetragonally elongated high-spin d^5 systems

Scheme 1 Structures of
Fe(TPP)X series of compounds
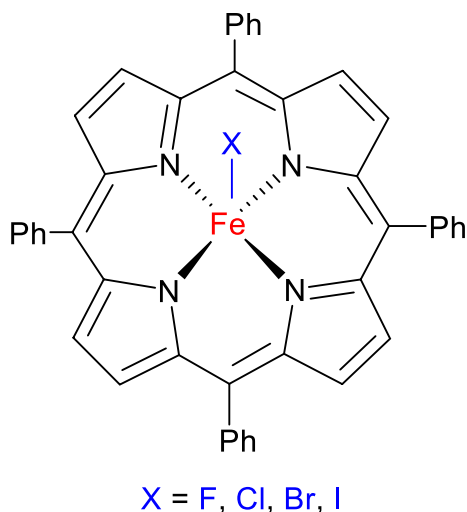
$$X = F, Cl, Br, I$$

such as Fe(TPP)X exhibit $D > 0$, but X plays a key role. Spin delocalization onto X means that there is a spin–orbit coupling (SOC) contribution to D from $X^\bullet$, as opposed to none from closed-shell X^-. Over the range X = F, Cl, Br, I, $X^\bullet$ character increases as does the intrinsic SOC of $X^\bullet$ so that D increases correspondingly over this range.

1 Introduction

Iron porphyrin complexes, especially those penta-coordinated, have been actively studied through the years [1–8], the interest being driven to a large degree by a desire to understand how heme proteins function [1–5]. In hemoglobin and myoglobin, penta-coordinated iron porphyrin(s) (hemin) use an open axial position to bind to O_2, thus transporting or storing oxygen in vertebrates. The porphyrins in metalloproteins typically have low symmetry due to their biosynthetically derived substituents, complicating their studies [9]. In contrast, synthetic porphyrins such as tetraphenylporphyrin are strictly fourfold symmetric and their iron complexes have been widely used as symmetrically substituted analogs and model compounds for myoglobin and hemoglobin [1–5]. These include five-coordinate tetraphenylporphyrinatoiron complexes such as $Fe^{III}(TPP)X$ (X = F, Cl, Br, I; TPP^{2-} = *meso*-tetraphenylporphyrinate dianion; Scheme 1) [8, 10–28].

Since the four equatorial nitrogen atoms in TPP^{2-} and the axial halide together exert a weak ligand field on the iron ion (i.e., the square pyramidal geometry being an extreme case of a tetragonally distorted octahedron), a key electronic feature of $Fe^{III}(TPP)X$ compounds is that they are high-spin: the five $3d$ electrons are all unpaired, yielding an $S = 5/2$ spin state. Their magnetic properties have been a subject of many studies [8, 10–21, 23–25, 27]. For example, the penta-coordinated hemes are also high-spin, and the unique binding between

hemoglobin and O_2 (with two unpaired electrons itself) is believed to be driven in part by the magnetic interactions between the two [29]. As with any high-spin ($S \geq 1$) system in sufficiently low symmetry, the Fe^{III} ion in complexes such as Fe^{III}(TPP)X undergoes the phenomenon of zero-field splitting (ZFS), where the interaction of the excited electronic states with the ground state mediated by the second-order spin–orbit coupling (SOC) leads to a splitting of otherwise degenerate m_S states (Scheme 1) [30]. (To a usually lesser degree, a direct interaction between the unpaired spins themselves, spin–spin coupling (SSC), also contributes to the ZFS.)

The ZFS provides a valuable window into the electronic structure of high-spin states, notably of transition-metal ions, but another of its aspects is as important, or perhaps even more important: the phenomenon of single-molecule magnetism. It is the ZFS that is responsible for the single-molecule magnet (SMM) behavior [31, 32] of such archetypal clusters as Mn_{12} [33–38] and Fe_8 [39–41]. The magnetic properties of the clusters are a result of single-ion ZFS of Mn^{III} and Mn^{IV} ions in the former [34, 42] and Fe^{III} in the latter [43]. More recently, single-molecular magnet properties were found in mononuclear complexes of, among others, $3d$ metal complexes [31, 44–69], including iron [46–56], that are often called single-ion magnets (SIMs). Of specific relevance, square pyramidal Fe^{III} complexes with intermediate spin ($S = 3/2$; as opposed to high-spin, $S = 5/2$) ground states have recently been shown to exhibit SIM properties [70].

Whichever of the above is the dominating motivation for studying iron porphyrins, accurately and precisely determining their ZFS is thus of utmost importance. Some of us dedicated a general review to the subject of how best to determine ZFS in metal complexes in general [71]. The series of Fe(TPP)X complexes presented in this work, however, offers a specific case which (a) allows one to compare diverse experimental techniques, including relatively new and advanced magnetic resonance methods such as High-Frequency and -Field EPR (HFEPR) and Far-Infrared Magnetic Spectroscopy (FIRMS), in terms of accuracy and precision of measurement and (b) from a scientific viewpoint, allows one to methodically track the influence of the axial halide ligand on the resulting ZFS of the given complex. To offer a brief historic background: of the current series, Fe(TPP)Cl has been by far the most investigated of the four compounds presented here by both magnetic resonance and non-resonance methods (Table 1 and references therein). Fe(TPP)Br has been the next-often researched member of the group while Fe(TPP)F and Fe(TPP)I have been only covered by some of us in previous work [24]. This past research will be discussed in more detail in the Sect. 4 of this work.

2 Experimental

Fe(TPP)F [28], Fe(TPP)Cl [72], Fe(TPP)Br [10], and Fe(TPP)I [72] were prepared by the literature methods. The syntheses of Fe(TPP)F [28], Fe(TPP)Br [10] and Fe(TPP)I [72] were described earlier [24].

Table 1 Spin Hamiltonian parameters of $Fe^{III}(TPP)X$ determined by different methods

Axial ligand	Method	D (cm^{-1})	E (cm^{-1})	$g_\perp$	$g_\parallel$	References
X = F	HFEPR	+4.67(1)	0.00(1)	1.97(1)	2.000(5)	This work
	INS	+4.49(9)	0			[24]
X = Cl	HFEPR	+6.458(2)	+0.015(5) $E/D = 0.002$	2.004(3)	2.02(1)	This work
	INS	+6.33(8)	0			[23]
	FD-FT THz-EPR	6.465	0.02 $E/D = 0.003$	2.0	1.95	[25]
	Far-IR	6.5				[8]
	VTVH MCD	6.9				[20]
	Magnetic Mössbauer	7(1)				[15]
	X-band EPR	3.2				[13]
	NMR	11.3				[11]
	Magnetic susceptibility	6.0(1)–11.9				[10, 14, 17, 18]
X = Br	HFEPR	+9.01(5)	+0.047(5) $E/D = 0.005$	1.99(1)	1.99(1)	This work
	FIRMS	+9.05		2.0	2.0	This work
	INS	+8.8(2)	0.1(2)			[24]
	Far-IR	9.15				[8]
	Magnetic susceptibility	4.9–12.5(5)				[10, 16, 19]
X = I	HFEPR	+13.84[a]	+0.07 $E/D = 0.005$	2.00	2.00	This work
	FIRMS	+13.95		2.0	2.0	This work
	INS	+13.4(6)	0.3(6)			[24]
	Magnetic susceptibility	13.5(5)				[19]

[a]The number of data points from the HFEPR spectra of Fe(TPP)I was not sufficient to do a proper least-square fit to yield an error estimate of the D and E values

2.1 HFEPR

HFEPR studies were performed at the National High Magnetic Field Laboratory (NHMFL, Tallahassee, FL, USA) and the Dresden High Magnetic Field Laboratory (HLD-EMFL, Dresden, Germany). The NHMFL EMR Facility operates a transmission spectrometer described elsewhere [73] modified by the use of Virginia Diodes Inc. (VDI, Charlottesville, VA, USA) sources, generating sub-THz wave radiation in a 50–640 GHz frequency range. The spectrometer is associated with a 15/17-T warm-bore superconducting magnet. HFEPR measurements at the HLD were performed at frequencies up to 750 GHz using a 16-T cold-bore magnet-based transmission-type multifrequency spectrometer (similar to that described earlier [74]) equipped with VDI sub-THz sources. In both cases, pellets made of *n*-eicosane and

the given compound as a powder in about ~ 30 mg quantity were used. Alternatively, the powder sample was immersed in an *n*-eicosane mull. The spectra were typically collected at 5–10 K in the NHMFL, and 2 K at HLD.

2.2 FIRMS

FIRMS spectra were collected at the NHMFL using a Bruker Vertex 80v FT-IR spectrometer coupled with a 17-T vertical-bore superconducting magnet in Voigt configuration. The experimental setup is equipped with a mercury lamp and a composite silicon bolometer (Infrared Laboratories), as an incoherent (sub)-THz radiation source and detector, respectively. Two gold-coated mirrors are used to guide the THz radiation from the spectrometer and to focus it onto the top of the probe. The mirrors are mounted inside the 7.6 cm (3 inch) diameter beamline which is evacuated to 3 mbar to eliminate strong parasitic absorption of water vapor. The radiation is then passed through the brass lightpipe [OD 1.9 cm (0.75 inch)] over a distance of 2.5 m from the source at room temperature to the field center part of the probe at low temperature. An *n*-eicosane pellet containing the powdered compound of interest (~ 7 mg) was measured in the spectral region between 5 and 50 cm^{-1} (0.15 − 1.5 THz) with a resolution of 0.3 cm^{-1} (9 GHz). Both sample and bolometer were cooled by low-pressure helium gas to ~ 4.5 K.

2.3 Spin Hamiltonian

ZFS is typically described by the spin Hamiltonian [30, 75]:

$$\hat{\mathcal{H}}_{ZFS} = D\left\{ \hat{S}_z^2 - \frac{1}{3}S(S+1)\hat{1} \right\} + E\left(\hat{S}_x^2 - \hat{S}_y^2 \right),\qquad(1)$$

where D and E are the axial and rhombic ZFS parameters, respectively, $\hat{S}_x$, $\hat{S}_y$, and $\hat{S}_z$ are the x, y, and z components of the spin operator, and $\hat{1}$ is the unitary operator.

Although higher-order terms can be considered in a spin Hamiltonian, e.g., fourth-order ZFS for $S \geq 2$ (such as the cubic ZFS terms denoted a or $B_4^{0,4}$) [75], we have not done so here as the zero-field data fits were sufficiently successful using only those terms given in Eq. (1). Fourth-order ZFS has been determined by HFEPR on powder samples in other cases [76].

For compounds with both molecular and crystallographic symmetries higher than twofold [30], the rhombic ZFS parameter E becomes zero and the spin Hamiltonian in Eq. (1) is simplified into Eq. (2), which now also includes the electronic Zeeman terms for an axial system. Analogous to the comment above for Eq. (1), higher-order Zeeman terms for $S \geq 3/2$ [77] are also possible, but were not considered as the parameters could be fitted to the field-dependent data sufficiently well without them:

$$\hat{\mathcal{H}} = D\left\{ \hat{S}_z^2 - \frac{1}{3}S(S+1)\hat{1} \right\} + \beta_e\left\{ g_\parallel B_z \hat{S}_z + g_\perp \left(B_x \hat{S}_x + B_y \hat{S}_y \right) \right\},\qquad(2)$$

where β_e is electron Bohr magneton (often given as μ$_B$), $g_\parallel$ and $g_\perp$ are the parallel (along the z axis) and perpendicular (in the xy plane) components of the g factor,

respectively, and B_x, B_y, and B_z are the x, y, and z components of the applied (external) magnetic field B_0.

The effect of the spin Hamiltonian (Eq. 2) acting on the $S=5/2$ wavefunction is depicted in Scheme 2 for positive D, which happens to be the case of all known iron(III) porphyrins, including the Fe(TPP)X series investigated in the current work. It should be noted that because of the Kramers theorem, all the $\pm m_S$ levels are degenerate in the absence of magnetic field, and this makes the $\pm 1/2$ pair of spin sublevels amenable to EPR at any frequency, particularly at X-band, as the transition between these sublevels is fully allowed ($\Delta m_S = \pm 1$), and its energy scales with field. This is the reason why X-band EPR has been such a historically successful technique to investigate hemes and hemoglobin, although it alone does not offer information on the ZFS of these systems.

3 Results

3.1 HFEPR

Fe(TPP)F produced a rich set of HFEPR spectra at low temperatures, and any frequency in the ~ 100–430 GHz range (Fig. 1, top left; see also Fig. S1, Supporting Information; a multifrequency collection of experimental spectra is shown in Fig. S2). The spectra could be adequately simulated using spin Hamiltonian parameters as in Fig. 1 caption and assuming a powder distribution of crystallites in the sample. The parameters, particularly the g-values, however, tended to be slightly frequency-dependent, as is usually the case in multi-frequency experiments. In order to obtain a frequency-independent set of parameters, a 2-D energy (or frequency) vs. magnetic field map of turning points was constructed, and the parameters fitted by a least-square method to the complete data set according to the tunable-frequency methodology (Fig. 2, top left) [78]. The resulting spin Hamiltonian parameters are found in Table 1. Most importantly, for Fe(TPP)F, the D-value is $+4.67(1)$ cm^{-1},

Scheme 2 The effect of spin Hamiltonian (Eq. 2) on an $S=5/2$ wavefunction. In high symmetry (higher than two-fold), as provided by the porphyrin ligand, $E=0$. An applied external magnetic field B_0 leads to additional splittings of the m_S levels due to the Zeeman effect
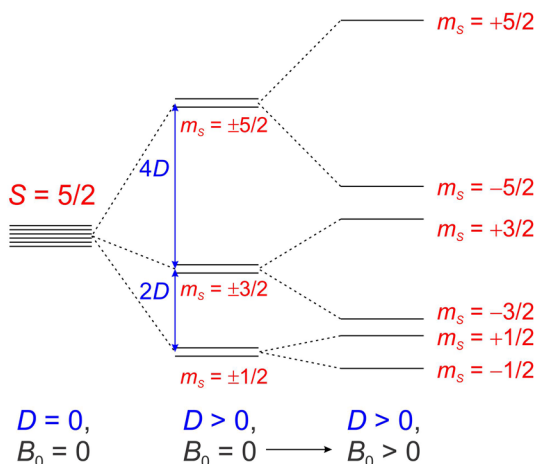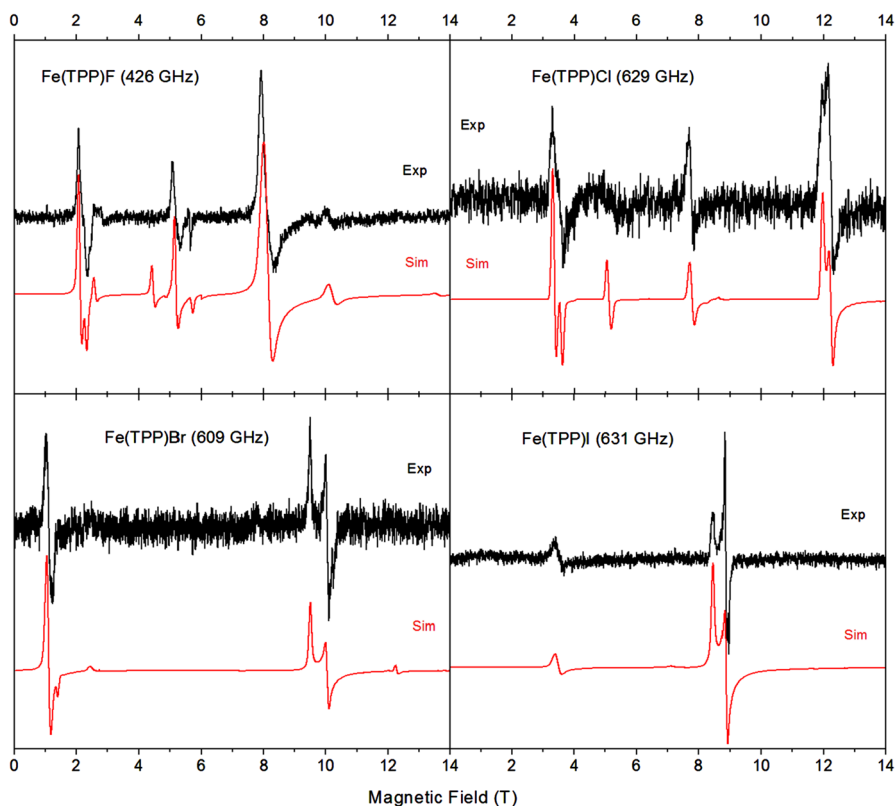
Fig. 1 Experimental HFEPR spectra at 5–10 K of the Fe(TPP)X series of compounds (black/upper traces) and their powder-pattern simulations (red/lower traces). Particular frequencies and spin Hamiltonian parameters used in the simulations are: Fe(TPP)F: frequency, 425.6 GHz, $D = +4.67$ cm^{-1}, $E = 0$, $g_{iso} = 1.97$; Fe(TPP)Cl: frequency, 628.8 GHz, $D = +6.458$ cm^{-1}, $E = +0.023$ cm^{-1}, $g = [2.01, 2.01, 2.00]$; Fe(TPP)Br: frequency, 609 GHz, $D = +9.01$ cm^{-1}, $E = +0.05$ cm^{-1}, $g = [1.98, 1.99, 1.99]$; Fe(TPP)I: frequency, 631 GHz, $D = +13.83$ cm^{-1}, $E = +0.07$ cm^{-1}, $g = [1.995, 1.995, 2.000]$ (the sign of E was in each case arbitrarily assigned as that of D). The splitting of the perpendicular intra-Kramers turning points (such as the one at 10 T in Fe(TPP)Br) is indicative of an exceedingly small ($E/D < 0.01$) yet measurable rhombicity of the ZFS tensor in each compound except Fe(TPP)F (color figure online)

while there is no detectable rhombicity of the ZFS tensor ($E = 0$); thus the complex symmetry remains perfectly fourfold.

Fe(TPP)Cl produced an EPR response of very high quality at any temperature from 5 to 200 K and above, and in a wide frequency range of 50–630 GHz (Fig. 1, top right; see also Figs. S3 and S4, Supporting Information). The experimental spectra could be well simulated and thanks to a small linewidth of the turning points, a minute E-value could be determined from the perpendicular resonances together with the D-value of $+6.458(2)$ cm^{-1}, which translates into a rhombicity factor E/D of the ZFS tensor as small as 0.002–0.003. This is an indication that the fourfold symmetry provided by the ligand is not exactly kept by the molecule in the solid state, similarly to the other members of the series except Fe(TPP)
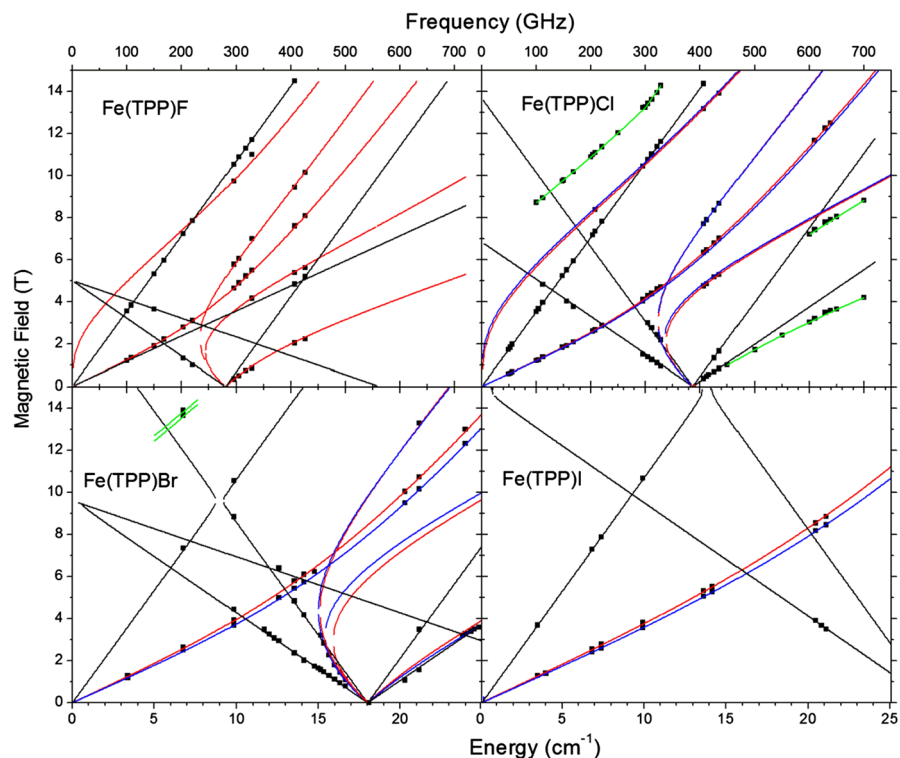
Fig. 2. 2-D field vs. energy (frequency) HFEPR maps of the Fe(TPP)X series of compounds. Squares are experimental turning points in the EPR powder spectra including the zero-field resonance in Fe(TPP) Br detected by FIRMS at 18.1 cm^{-1}; curves are simulations using spin Hamiltonian parameters as in Table 1. Red curves: simulations with magnetic field parallel to the *x*-axis of the ZFS tensor; blue curves: $B_0 \parallel y$ axis, black curves: $B_0 \parallel z$ axis, green curves: off-axis turning points in Fe(TPP)Cl and Fe(TPP)Br. Only those simulated turning points were plotted that show experimental points on them; others were omitted for clarity. For Fe(TPP)Cl, the splitting of the perpendicular turning points is smaller than the symbol size. For that reason, only one set of perpendicular experimental data points is shown (color figure online)

F. The final frequency-independent spin Hamiltonian parameters were obtained from a 2-D map similarly to Fe(TPP)F (Fig. 2, top right) and are to be found in Table 1.

The EPR response of the third complex of the series, Fe(TPP)Br, was almost as good as those of the two previously described analogs. Figure 1 (bottom left) shows a typical spectrum accompanied by powder-pattern simulations using spin Hamiltonian parameters as in the figure caption. Another spectrum, obtained at a lower frequency, is shown in Fig. S5 in the Supporting Information and additional multifrequency spectra in Fig. S6. The axial ZFS parameter *D* was established at +9.01 cm^{-1} and the very small rhombicity of the ZFS tensor ($E/D \sim 0.005$) shows in the visible splitting of the perpendicular turning point of the intra-Kramers transition at 10 T. The final frequency-independent spin Hamiltonian

parameters were obtained as before from a 2-D map of turning points shown in (Fig. 2, bottom left) and are to be found in Table 1.

Finally, the fourth complex, Fe(TPP)I also generated informative HFEPR spectra. Figure 1 (bottom right) shows one of these spectra accompanied by powder-pattern simulations using spin Hamiltonian parameters as in the figure caption. The axial ZFS parameters D was found to be $+13.84$ cm^{-1} and a minute rhombicity ($E/D \sim 0.005$) of the ZFS tensor shows in the visible splitting of the perpendicular turning point of the intra-Kramers transition at 9 T. Another spectrum, obtained at a lower frequency, is shown in Fig. S7 in the Supporting Information with a multi-frequency collection of experimental spectra shown in Fig. S8. The final frequency-independent spin Hamiltonian parameters were obtained as before from a 2-D map of turning points shown in (Fig. 2, bottom right) and are to be found in Table 1. Note that although the highest HFEPR operating frequency (631 GHz, 21 cm^{-1}) was significantly lower than the 2|D| energy gap (27.9 cm^{-1}, see the Sect. 3.2 below), an observation of the inter-Kramers turning points such as the one visible at 3.5 T in the corresponding spectrum made it possible to obtain the D-value for Fe(TPP)I independent of FIRMS.

3.2 FIRMS

FIRMS has been used extensively to probe magnetic transitions in metal complexes with large zero-field splitting [8, 66, 79–86]. The great advantage of Fourier-transform spectroscopy is being able to cover the broad spectral range where transitions between zero-field energy levels might be observed. The application of the magnetic field gives the second variable for plotting the absorption spectrum in two dimensions, although significant costs are paid in terms of THz wave radiation power reaching the sample. Two spectra of the THz radiation transmitted through the sample were recorded for each magnetic field to estimate the signal-to-noise ratio. The magnetic resonance absorption spectrum is obtained as $A = 1 - T$, where T is the ratio between the THz transmission measured at each magnetic field and a reference spectrum. The latter is the average THz transmission for all magnetic fields. This approach allows one to distinguish field-dependent absorption among the field-independent spectral features, such as vibrational modes and instrumental function.

The experimental FIRMS spectra shown in Fig. 3 in a form of 2-D maps (field vs. energy) were analyzed and simulated using an in-house written program based on the EasySpin toolbox [87]. This toolbox was originally developed for the analysis of magnetic resonance absorption in the field domain, but also provides a capability for calculations of the magnetic-dipole transition probability in the frequency domain. The effect of random orientation of the microcrystallites in the powder is taken into account and Lorentzian line broadening added to obtain the final simulated spectrum.

The lowest limit of the FIRMS spectral range is essential for spectroscopic studies of SMMs and is defined by the design of the particular experimental set-up. The intensity of the THz radiation emitted by a broadband thermal source is
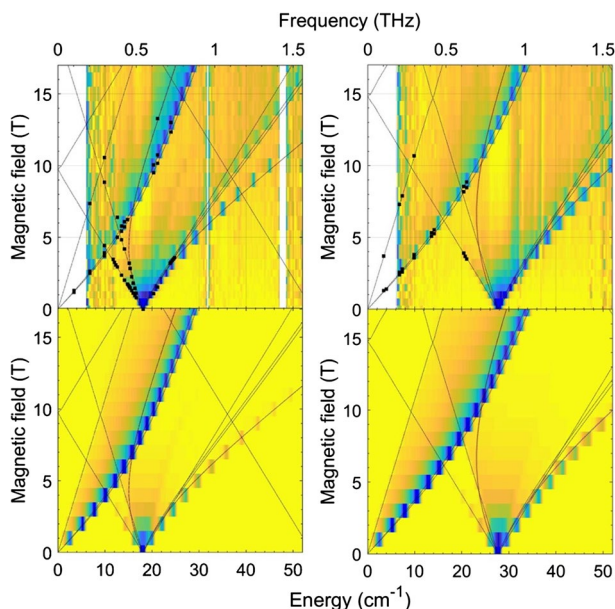
Fig. 3 (Top left) 2-D map of magnetic resonance absorption (also called FIRMS) in Fe(TPP)Br at 4.6 K with HFEPR data points added as black squares. A zero-field transition is clearly visible at 18.1 cm^{-1} representing the transition between the $\pm 1/2$ and $\pm 3/2$ Kramers doublets. The intra-Kramers transition within the $\pm 1/2$ manifold is also visible at higher fields (4–17 T) in the low-energy region (10–24 cm^{-1}). The lines are simulations of all possible turning points (including those of nominally forbidden transitions) in the powder spectrum using: $D = +9.05$ cm^{-1}, $E = +0.05$ cm^{-1}, $g_{iso} = 2.0$ (g_{iso} is the isotropic g factor). (Top right) 2-D map of magnetic resonance absorption in Fe(TPP)I. A zero-field transition is clearly visible at 27.9 cm^{-1} representing the transition between the $\pm 1/2$ and $\pm 3/2$ Kramers doublets. The intra-Kramers transition within the $\pm 1/2$ manifold is also visible at higher fields (4–17 T) in the low-energy region (10–30 cm^{-1}). The lines are simulations of turning points in the powder spectrum using $D = +13.95$ cm^{-1}, $E = +0.07$ cm^{-1}, $g_{iso} = 2.0$. (Bottom) Simulated maps for the respective compounds. The false-color simulation reproduces the allowed ($\Delta m_S = \pm 1$) transitions only, as different from the lines. That nominally forbidden resonances such as $|-1/2\rangle = |+3/2\rangle$ appear in the experimental maps (the top two windows), is most likely due to the presence of a $B_1 \parallel B_0$ component in the THz radiation (B_1 is the magnetic, as opposed to electrical, field of the applied radiation) in addition to the standard $B_1 \perp B_0$ one (color figure online)

about 0.05% compared to mid-infrared range, which commercial FT-IR spectrometers are generally tailored to. The typical sensitivity of FIRMS measurements at NHMFL drops precipitously below 15 cm^{-1} (Fig. S9 in Supporting Information). This was one of the reasons why, of the four Fe(TPP)X complexes, only Fe(TPP) I and Fe(TPP)Br were addressed by the FIRMS technique, since the ZFS energies of Fe(TPP)F and Fe(TPP)Cl were fully determined by HFEPR. Nevertheless, a low-frequency resonance absorption at 10 cm^{-1} (0.3 THz) can still be observed in both Fe(TPP)Br and Fe(TPP)I. This relatively strong (~30%) absorption corresponds to the transition within the $m_S = \pm 1/2$ Kramers doublet and confirms the positive sign of D for both compounds. The quality of these spectra is essentially the same as those of the FD-FT THz-EPR (Frequency-Domain Fourier-Transform

Terahertz-EPR) studies on Fe(TPP)Cl reported by the BESSY II facility in Berlin [25]. Despite the difference in terminology, their instrumental approach is basically the same as ours in terms of employing a Bruker FT-IR spectrometer. However, their spectrometer is coupled to an optical split-coil magnet, which yields sensitivity benefits due to the free-space propagation of the THz radiation and its direct incidence on the sample. A key difference of course is that BESSY II can also use coherent synchrotron radiation in the THz region as described elsewhere [88].

4 Discussion

4.1 Overview of the ZFS in Fe(TPP)X

The most-researched complex of the Fe(TPP)X series has been Fe(TPP)Cl, its ZFS studied by a variety of experimental and theoretical methods, including magnetic susceptibility measurements [10, 14, 17, 18], Fourier-Transform Frequency-Domain (FT-FD) THz- and HF-EPR [25], inelastic neutron scattering (INS) [23], far-IR [8], Mössbauer spectroscopy [15], magnetic circular dichroism (MCD) [20], solution NMR [11], and X-band EPR [13]. It thus offers an excellent object for discussing the merits of particular techniques.

The most convenient (i.e., accessible) and least expensive method, dc magnetic susceptibility measurement as a function of temperature, is still the most widely used [89]. This technique, however, suffers from a number of extrinsic, practical considerations that can adversely affect the results: inaccuracy in sample mass (especially where sample quality is limited), insufficient diamagnetic corrections, ferromagnetic impurities (particularly for Fe-containing systems, where there can be Fe nanoparticle impurities) or other experimental problems such as a drift in the centering of the sample within the field. As an example of these difficulties in the present system, the reported D values for Fe(TPP)Cl from such measurements cover a very large range of energies: 6.0(1)–11.9 cm^{-1} [10, 14, 17, 18]. While the lower end of these values is close to the true value as determined by direct methods like HFEPR or FIRMS, the upper end is about 100% off. The Fe(TPP)Br analog was also studied by magnetic susceptibility [10, 16, 19], with the resulting ZFS parameters widely varying on the energy scale from about 50% undervalued to 30% overvalued. Also note that in neither case was the magnetic susceptibility data analysis hampered by any degree of ZFS rhombicity, as is often the case in other spin systems. This indirect technique is thus generally not accurate and should be treated with utmost skepticism when evaluating ZFS.

Interestingly, the early far-IR studies of Fe(TPP)Cl and Fe(TPP)Br by Uenoyama in 1971 [8], which were performed using a home-made Michelson interferometer that Richards, Brackett and coworkers had developed [6, 7, 90], offered accurate if not precise values for both compounds. A modern extension of this technique which different groups practicing it call FD-FT THz-EPR or FIRMS offers an improved accuracy and precision, particularly when complemented by HFEPR. It is particularly gratifying to see the almost perfect agreement between the ZFS parameters in Fe(TPP)Cl obtained by FD-FT THz-EPR at the BESSY II facility in Berlin [25]

with those delivered by HFEPR at the NHMFL in Tallahassee (this work). Equally good agreement was achieved between HFEPR and FIRMS, both as performed within this work on Fe(TPP)Br and Fe(TPP)I.

A non-magnetic resonance method, Inelastic Neutron Scattering (INS) [91–95], has been practiced to measure ZFS in a variety of high-spin metal ions [23, 24, 35, 36, 40, 83, 96–113]. It was employed previously by some of us on the same series of Fe(TPP)X compounds reported in this work [23, 24]. Because the INS experiments for Fe(TPP)X were not conducted with an external magnet [23, 24], they did not deliver the g-values of the system under study. This, however, is not a problem for the Fe(TPP)X series in which the g-values of the Fe^{III} ion are consistently very close to 2.00. Otherwise, INS delivers very robust values of the ZFS parameters in agreement with magnetic resonance. There are two features of INS that make it advantageous to probe magnetic transitions in molecular compounds: (1) It offers a unique dependence of the magnetic transitions on the neutron scattering angles (or momentum transfer Q), whether or not the INS experiments are conducted with an external magnet. This angular dependence was used to distinguish the magnetic transitions from those of phonons in the INS spectra of Fe(TPP)X (X = F, Cl, Br, I) [23, 24]. Thus, although INS is typically used in zero field, it can provide the needed discrimination between magnetic and vibrational (non-magnetic) signals. Since Q is a vector, 4D-INS (i.e., dimensions of Q_x, Q_y, Q_z, and E = energy of the neutrons scattered from the sample) has been used recently to probe magnetic exchange interactions, spin dynamics, and the entanglement between molecular qubits in metal complexes [38, 114–116]. (2) INS experiments can also be conducted with external magnets [83, 84, 104] to probe both intra-Kramers ($m_S = -1/2 \rightarrow +1/2$) [104] and inter-Kramers doublet transitions in transition-metal and lanthanide SIMs [83, 84]. For example, INS spectra of Co(acac-d_7)$_2$(D$_2$O)$_2$ (acac = pentane-2,4-dionate anion) at 0–10 T on the direct-geometry, time-of-flight Disk-Chopper Spectrometer (DCS) [95] revealed both $m_S = -1/2 \rightarrow +1/2$ and $m_S = \pm 1/2 \rightarrow \pm 3/2$ transitions [104], offering comparisons with the results from other studies [85, 117]. The intra-Kramers ($m_S = -1/2 \rightarrow +1/2$) transition at 0–10 T was simulated with D, E, and g values from an earlier work [117]. Another difference between the variable-temperature (VT) INS and HFEPR/FIRMS spectroscopies of Fe(TPP)X (X = F, Cl, Br, I) is that the INS spectra showed both the lower energy, $m_S = \pm 1/2 \rightarrow \pm 3/2$ absorptions (at 2D in the range of 9.5–27.4 cm^{-1}) and the higher energy, $m_S = \pm 3/2 \rightarrow \pm 5/2$ absorptions (at 4D in the range of ~ 18–55 cm^{-1}) at 10–100 K [23, 24]. In addition, the transitions from the excited $m_S = \pm 3/2$ states to the ground $m_S = \pm 1/2$ states were also observed in the VT-INS spectra of all four Fe(TPP)X complexes [23, 24]. For Fe(TPP)F and Fe(TPP)Br at 50 K when the highest energy ZFS states $m_S = \pm 5/2$ (Scheme 2) are sufficiently populated, the $m_S = \pm 5/2 \rightarrow \pm 3/2$ transitions (at 4D) were also observed [23, 24]. In such "emission" INS spectra, the neutrons scattered by the samples gain energy. For comparison, HFEPR and FIRMS spectra of the complexes in the current work were conducted at 2–10 and 4.6 K, respectively, when just the ground $m_S = \pm 1/2$ states were populated. Thus, these two spectroscopies essentially probed the $m_S = \pm 1/2 \rightarrow \pm 3/2$ absorptions (at 2D).

A very small offset on the order of 2–4% in the D-values obtained by INS, in comparison to those obtained from magnetic resonances, persists for all complexes

reported in this work (Table 1), which we are not yet able to explain. As pointed out earlier, the D-values from INS were from simulation of the spectra at zero magnetic field [23, 24], while those from magnetic resonances (HFEPR and FIRMS) are from simulations of the spectra collected in magnetic fields. In addition, the simulations of INS spectra involved the "emission" peaks as well as the higher energy, $m_S = \pm 3/2 \rightarrow \pm 5/2$ absorptions in Fe(TPP)X (X = F, Br, I) [23, 24].

Of other experimental techniques, both Mössbauer and MCD spectroscopies deliver dependable and accurate values of ZFS parameters, albeit without the precision of magnetic resonance, and with Mössbauer requiring an external magnetic field and being essentially limited to Fe-containing systems [118]. The indirect methods such as X-band EPR and solution NMR lead to very large errors and should generally be avoided for the purpose of evaluating ZFS.

4.2 Understanding the ZFS in Fe(TPP)X

The recent INS and ab initio studies by some of us [23, 24] to calculate D and E values of all four complexes Fe(TPP)X were a comprehensive investigation of the iron porphyrin halides. The origin of the large and positive D-values of the $^6A_1$ ground state in Fe(TPP)X was studied by the complete active space self-consistent field (CASSCF) and the N-electron valence perturbation theory (NEVPT2), reproducing the trends of D from INS [24]. The results showed a correlation between the increase of the D-values and decrease of the π- and σ-antibonding energies (e_π^X and e_σ^X) of the Fe–X bonds from X = F to I.

We believe that a much simpler model based on Ligand Field Theory (LFT) could also explain at least semi-quantitatively the trend of increasing ZFS along the series of axial ligands, from F to Cl to Br and to I. Of particular instruction might be a comparison with an analogous series of tetraporphyrinato halide compounds with a different metal ion, Mn^{III} ($3d^4$), where the trend is exactly reversed [105]. This approach has already been used, by Gatteschi and Sorace for distorted octahedral complexes [119], specifically for both high-spin Fe^{III} and other high-spin ions, namely high-spin Mn^{III} ($3d^4$, $S = 2$) [120], perhaps most widely studied by HFEPR [71, 120, 121], as well as other techniques, including INS [23, 24]. In the case of Mn^{III}, it is clear that, barring any complications from non-innocent (especially heavy atom) ligands [122], $D < 0$ corresponds to axial (tetragonal) elongation, as is the case for Mn(TPP)Cl [105], and $D > 0$ to axial compression [123]. This situation for Mn^{III} is relatively simple because the ZFS is dominated by SOC involving excited states within the ground-state free-ion ^5D ($L = 2$, $S = 2$) manifold. The D value depends on the ligand-field energy splitting as follows (Eq. 3) [124]:

$$D = \lambda^2 \left(-\frac{4}{\Delta} + \frac{1}{\Delta - \delta_1} - \frac{4}{\delta_3} \right), \tag{3}$$

where Δ is the octahedral splitting, δ_1 is the tetragonal splitting, which is basically the energy difference between the d_{xy} and d_{xz}/d_{yz} orbitals (degenerate in C_{4v} symmetry), and δ_3 is the energy of the most relevant (among many) triplet excited state (derived from $^3T_{1g}(^3H)$, $t_2^4 e^0$).

In contrast, for Fe^{III}, there is no SOC within the ground state free-ion ^{6}S manifold as $L = 0$. The ZFS results from mixing via SOC of primarily excited quartet states, of which there are many, even in high symmetry (i.e., O_h point-group): ^{4}T$_{1g}$(^{4}G, ^{4}F, ^{4}P), ^{4}T$_{2g}$(^{4}G, ^{4}F, ^{4}D), ^{4}E$_g$(^{4}G, ^{4}D), ^{4}A$_{1g}$(^{4}G), and ^{4}A$_{2g}$(^{4}F). Most of these, however, are at very high energy with respect to the ^{6}A$_{1g}$(^{6}S) (in O_h) sextet ground state ($t_2^3 e^2$ in strong-field notation) and can be disregarded in a simple approach. This can be shown by an exact calculation using the matrix elements given by McClure [125] and the parameters used by Gatteschi and Sorace [119]: Racah parameters $B = 536$ cm^{-1}, $C = 3260$ cm^{-1}, and $Dq = 1500$ cm^{-1} (roughly the average of the axial and equatorial octahedral splitting they used). This gives the ^{4}T$_{1g}$(^{4}G) excited state ($t_2^4 e^1$) lying at ~ 9400 cm^{-1} above the ^{6}A$_{1g}$(^{6}S) ground state and the ^{4}T$_{2g}$(^{4}G) excited state (also $t_2^4 e^1$) lying at ~ 13,040 cm^{-1}. It should be noted that Paulat and Lehnert saw evidence in the MCD and UV–Vis–NIR spectra of Fe(TPP)Cl for these transitions at 11,584 and 13,542 cm^{-1}, respectively [28]. All the other spin quartet excited states lie greater than ~ 22,000 cm^{-1} above the ground state. The many spin doublet excited states are also at > 20,000 cm^{-1} above the ground state, and most are much higher in energy. There is one low-lying doublet excited state, ^{2}T$_{2g}$(^{2}I) ($t_2^5 e^0$), but this requires a double-spin-flip to connect to the ground state, which is not allowed. The calculations by Gatteschi and Sorace showed that, similar to Mn^{III}, tetragonal elongation gave one sign of D and compression the other, but oppositely so [and more than an order of magnitude smaller, as $|D| = 4.75(5)$ cm^{-1} for Mn^{III}] in that elongation gave $D \approx +0.3$ cm^{-1} and compression gave $D \approx -0.3$ cm^{-1}. In the case of Fe(TPP)X, however, due to the five-coordinate (square pyramidal) geometry, the situation is always one of tetragonal elongation, and indeed, the positive sign of D reported for these complexes (Table 1) is consistent with this simple model. The following LFT expression helps to demonstrate this behavior (Eq. 4) [75]:

$$D = \frac{1}{10}\zeta^2 \left(\frac{2}{E_z} - \frac{1}{E_x} - \frac{1}{E_y} \right) = \frac{1}{5}\zeta^2 \left(\frac{1}{E\left(^4A_2\left(^4T_{1g}\right)\right)} - \frac{1}{E\left(^4E\left(^4T_{1g}\right)\right)} \right), \quad (4)$$

where E_i, $i = x, y, z$, corresponds to the energies for excited states that involve pairing of the electron in the d_{x2-y2} (highest energy) orbital of the sextet ground state into the d_{yz}, d_{xz}, and d_{xy} orbitals, respectively. The second part of the equation is that given in the earlier ab initio studies by Stavretis et al. [24] and is suited to the axial symmetry found here, with the symmetry designations of the states derived from the ^{4}T$_{1g}$(^{4}G) excited state mentioned above. Due to π-bonding with the axial halido ligand, the ^{4}E state (i.e., $d_{xy}^1 d_{yz}^1 d_{xz}^2 d_{z2}^1$ / $d_{xy}^1 d_{yz}^2 d_{xz}^1 d_{z2}^1$) is higher in energy than the ^{4}A$_2$ state (i.e., $d_{xy}^2 d_{yz}^1 d_{xz}^1 d_{z2}^1$) so D is positive.

These simple (i.e., d^n only, $n = 4, 5$) LFT models work well for complexes wherein all of the ligands are light atoms. The difficulty is when the ligand, in this case the axial halido ligand, has both some non-innocent character and a large intrinsic SOC. The first point means that the traditional oxidation state assignment/electronic configuration of a Group 17 ligand as closed shell X$^-$: [N.G.]$ns^2 np^6$ (and likewise, a Group 16 ligand as E^{2-}: [N.G.]$ns^2 np^6$, etc.) is not

a truly appropriate description, but the ligand may instead have atomic/radical character (i.e., $X^{\bullet 0}$: [N.G.]ns^2np^5, and Group 16 as $E^{\bullet-}$: [N.G.]ns^2np^5, etc.). The second point stems from the fact that the SOC constants of the Group 17 elements in their neutral atom state, i.e., [N.G.]np^5 electronic configuration ($^2P_{3/2}$), increases as follows (in cm^{-1}): F^0, 269.3; Cl^0, 588.2; Br^0, 2328.8; I^0, 5068.6 [126]. For fluorine, non-innocence is decidedly not the case, neither for chlorine, but for bromine, and in particular iodine, the complexes can be described to some extent as "resonance forms" of [$Fe^{III}(TPP^{2-})X^-$] and [$Fe^{II}(TPP^{2-})X^{\bullet 0}$] (X = Br, I). This was the situation encountered by Mossin et al. for a *trans*-bisiodido Mn^{III} cyclam (cyclam = 1,4,8,11-tetraazacyclotetradecane) complex [122], wherein [$Mn^{III}(cyclam^0)(I^-)_2$]$^+$ ↔ [$Mn^{III}(cyclam^0)(I^-)(I^{\bullet 0})$]$^+$ (i.e., $[(5p^6)(d_{xy}^{1}d_{yz}^{1}d_{xz}^{1}d_{z2}^{1}) \leftrightarrow (5p^5)(d_{xy}^{1}d_{yz}^{1}d_{xz}^{1}d_{z2}^{2}) \leftrightarrow (5p^5)(d_{xy}^{1}d_{yz}^{1}d_{xz}^{2}d_{z2}^{1}) \leftrightarrow (5p^5)(d_{xy}^{1}d_{yz}^{2}d_{xz}^{1}d_{z2}^{1})]$) is minimally operative. This behavior is of course enhanced by the presence of *two* iodido ligands, which are involved in both σ-bonding (charge transfer into Mn d_{z2} orbital) and π-bonding (charge transfer into Mn d_{xz} or d_{yz} orbitals). In a *tour-de-force* of ligand-field theory, Mossin et al. showed that the ZFS was positive due to this large SOC constant of iodine that makes a net *positive* contribution to D [122]. Qualitatively, the same effect is seen in the Mn(TPP)X series, wherein Mn(TPP)Cl has ZFS that is typical for Mn^{III} in a tetragonally elongated environment (D = −2.26(3) cm^{-1}), while for Mn(TPP)Br, the ZFS has changed substantially (D = −1.09 cm^{-1}), and for Mn(TPP)I, it has shifted to "the other side": D = +1.3 cm^{-1}. What about [Fe(TPP)X]? Fe^{III} would be expected to be a stronger Lewis acid than Mn^{III} and thus [$Fe^{III}(TPP^{2-})X^-$] ↔ [$Fe^{II}(TPP^{2-})X^{\bullet 0}$] (X = Br, I) should be at least as relevant as in the cyclam complex. The question is, how does the right-side "resonance form" contribute to D, positively or negatively? The method used by Mossin et al. is currently beyond our capabilities and is likely even more challenging for the Fe^{III} case as the operative electronic configurations have another electron: $[(5p^6)(d_{xy}^{1}d_{yz}^{1}d_{xz}^{1}d_{z2}^{1}d_{x2-y2}^{1}) \leftrightarrow (5p^5)(d_{xy}^{1}d_{yz}^{1}d_{xz}^{1}d_{z2}^{2}d_{x2-y2}^{1}) \leftrightarrow (5p^5)(d_{xy}^{1}d_{yz}^{1}d_{xz}^{2}d_{z2}^{1}d_{x2-y2}^{1}) \leftrightarrow (5p^5)(d_{xy}^{1}d_{yz}^{2}d_{xz}^{1}d_{z2}^{1}d_{x2-y2}^{1})]$. All that we can propose here is that the net contribution of SOC from the axial halido ligand is positive in this high-spin d^5 case as well, so that the positive D value that obtains for the innocent electronic configuration, $(5p^6)(d_{xy}^{1}d_{yz}^{1}d_{xz}^{1}d_{z2}^{1}d_{x2-y2}^{1})$, is overall added to by the contributions from the non-innocent ones. Thus, a positive D value always obtains for Fe(TPP)X, but increases smoothly in magnitude as one moves down the Group 17 elements; indeed, a plot of D values of Fe(TPP)X ersus Z_X (atomic number of the halides X) is linear with $R^2 = 0.98$; Fig. S10 in Supporting Information. Given that the behavior of the axial halido ligand is essentially the same in Fe(TPP)X as in [Mn(tetraaza-macrocycle)X]$^{m+}$ (m = 0, 1) this analogous behavior is plausible.

5 Conclusions

The current HFEPR and FIRMS studies of the important series of axially halide-coordinated square pyramidal iron(III) porphyrins, Fe(TPP)X (X = F, Cl, Br, I) have probed intra- and inter-Kramers doublet magnetic transitions in these S = 5/2

complexes, yielding the spin Hamiltonian parameters: ZFS (*D* and *E*) and *g* values. These parameters have been compared with those from earlier spectroscopic and magnetic studies and show the high level of accuracy and precision available from the combination of field-domain (i.e., HFEPR) and frequency-domain (i.e., FIRMS) magnetic resonance techniques. Other spectroscopic techniques, such as applied field Mössbauer and VTVH-MCD can yield reliable spin Hamiltonian parameters and other useful information as well, such as ^{57}Fe hyperfine coupling constants via the former [118] and electronic transition information via the latter technique [28]. In contrast, magnetic susceptibility, while easy and readily available, is less reliable for yielding high accuracy information on spin Hamiltonian parameters. The *D* values (in cm^{-1}) in the Fe(TPP)X series increase smoothly as follows: $+4.67(1)$ (X$=$F), $+6.458(2)$ (X$=$Cl), $+9.05$ (X$=$Br), $+13.95$ (X$=$I). A qualitative model based on LFT explained this trend by attributing it to the combination of increasing spin delocalization from Fe onto the X ligand coupled with the large increase in atomic SOC constant as the halogen atomic number increases over the range from F to I.

Compliance with ethical standards

Conflict of interest The authors declare no conflicts of interest.

References

1. D. Dolphin, *The Porphyrins* (7 volumes), (Academic Press, New York, 1978–1979)
2. K.M. Kadish, K.M. Smith, R. Guilard, *The Porphyrin Handbook* (20 volumes), (Academic Press, San Diego, 2000–2003)
3. K.M. Kadish, K.M. Smith, R. Guilard, *Handbook of Porphyrin Science with Applications to Chemistry* (Physics, Materials Science, Engineering, Biology and Medicine, World Scientific, Singapore, Starting in, 2010)
4. F.A. Walker, Coord. Chem. Rev. **185–186**, 471–534 (1999). https://doi.org/10.1016/S0010-8545(99)00029-6
5. F.A. Walker, Chem. Rev. **104**, 589–616 (2004). https://doi.org/10.1021/cr020634j
6. P.L. Richards, W.S. Caughey, H. Eberspaecher, G. Feher, M. Malley, J. Chem. Phys. **47**, 1187–1188 (1967). https://doi.org/10.1063/1.1712038

7. G.C. Brackett, P.L. Richards, W.S. Caughey, J. Chem. Phys. **54**, 4383–4401 (1971). https://doi.org/10.1063/1.1674688
8. H. Uenoyama, Biochim. Biophys. Acta **230**, 479–481 (1971). https://doi.org/10.1016/0304-4165(71)90176-0
9. J.S. Lindsey, in *The Porphyrin Handbook*, ed. by K.M. Kadish, K.M. Smith, R. Guilard (Academic Press, San Diego, 2000), pp. 45–118
10. C. Maricondi, W. Swift, D.K. Straub, J. Am. Chem. Soc. **91**, 5205–5210 (1969). https://doi.org/10.1021/ja01047a003
11. G.N. La Mar, G.R. Eaton, R.H. Holm, F.A. Walker, J. Am. Chem. Soc. **95**, 63–75 (1973). https://doi.org/10.1021/ja00782a012
12. M. Sato, H. Kon, Inorg. Chem. **14**, 2016–2018 (1975). https://doi.org/10.1021/ic50150a060
13. M. Sato, A.S. Rispin, H. Kon, Chem. Phys. **18**, 211–224 (1976). https://doi.org/10.1016/0301-0104(76)87048-6
14. D.V. Behere, V.R. Marathe, S. Mitra, J. Am. Chem. Soc. **99**, 4149–4150 (1977). https://doi.org/10.1021/ja00454a040
15. D.H. Dolphin, J.R. Sams, T.B. Tsin, K.L. Wong, J. Am. Chem. Soc. **100**, 1711–1718 (1978). https://doi.org/10.1021/ja00474a011
16. D.V. Behere, S.K. Date, S. Mitra, Chem. Phys. Lett. **68**, 544–548 (1979). https://doi.org/10.1016/0009-2614(79)87257-7
17. D.V. Behere, S. Mitra, Inorg. Chem. **18**, 1723–1724 (1979). https://doi.org/10.1021/ic50196a066
18. D.V. Behere, S. Mitra, Indian J. Chem. **19A**, 505–507 (1980)
19. D.V. Behere, R. Birdy, S. Mitra, Inorg. Chem. **20**, 2786–2789 (1981). https://doi.org/10.1021/ic50223a009
20. W.R. Browett, A.F. Fucaloro, T.V. Morgan, P.J. Stephens, J. Am. Chem. Soc. **105**, 1868–1872 (1983). https://doi.org/10.1021/ja00345a032
21. H.M. Goff, E.T. Shimomura, M.A. Phillippi, Inorg. Chem. **22**, 66–71 (1983). https://doi.org/10.1021/ic00143a017
22. F. Paulat, V.K.K. Praneeth, C. Näther, N. Lehnert, Inorg. Chem. **45**, 2835–2856 (2006). https://doi.org/10.1021/ic0510866
23. S.C. Hunter, A.A. Podlesnyak, Z.-L. Xue, Inorg. Chem. **53**, 1955–1961 (2014). https://doi.org/10.1021/ic4028354
24. S.E. Stavretis, M. Atanasov, A.A. Podlesnyak, S.C. Hunter, F. Neese, Z.-L. Xue, Inorg. Chem. **54**, 9790–9801 (2015). https://doi.org/10.1021/acs.inorgchem.5b01505
25. J. Nehrkorn, J. Telser, K. Holldack, S. Stoll, A. Schnegg, J. Phys. Chem. B **119**, 13816–13824 (2015). https://doi.org/10.1021/acs.jpcb.5b04156
26. E.S. Ryland, M.-F. Lin, M.A. Verkamp, K. Zhang, K. Benke, M. Carlson, J. Vura-Weis, J. Am. Chem. Soc. **140**, 4691–4696 (2018). https://doi.org/10.1021/jacs.8b01101
27. C. Römelt, S. Ye, E. Bill, T. Weyhermüller, M. van Gastel, F. Neese, Inorg. Chem. **57**, 2141–2148 (2018). https://doi.org/10.1021/acs.inorgchem.7b03018
28. F. Paulat, N. Lehnert, Inorg. Chem. **47**, 4963–4976 (2008). https://doi.org/10.1021/ic8002838
29. S.A. Wilson, T. Kroll, R.A. Decreau, R.K. Hocking, M. Lundberg, B. Hedman, K.O. Hodgson, E.I. Solomon, J. Am. Chem. Soc. **135**, 1124–1136 (2013). https://doi.org/10.1021/ja3103583
30. R. Boča, Coord. Chem. Rev. **248**, 757–815 (2004). https://doi.org/10.1016/j.ccr.2004.03.001
31. C. Benelli, D. Gatteschi, in *Introduction to Molecular Magnetism* (Wiley-VCH, Weinheim, 2015) pp. 217−237
32. E.J.L. McInnes, R.E.P. Winpenny, in *Comprehensive Inorganic Chemistry II*, ed. by K. Poeppelmeier (Elsevier, Amsterdam, 2013), pp. 371–395
33. R. Sessoli, D. Gatteschi, A. Caneschi, M.A. Novak, Nature **365**, 141–143 (1993). https://doi.org/10.1038/365141a0
34. A. Caneschi, D. Gatteschi, R. Sessoli, A.L. Barra, L.C. Brunel, M. Guillot, J. Am. Chem. Soc. **113**, 5873–5874 (1991). https://doi.org/10.1021/ja00015a057
35. Y. Zhong, M.P. Sarachik, J.R. Friedman, R.A. Robinson, T.M. Kelley, H. Nakotte, A.C. Christianson, F. Trouw, S.M.J. Aubin, D.N. Hendrickson, J. Appl. Phys. **85**, 5636–5638 (1999). https://doi.org/10.1063/1.369824
36. I. Mirebeau, M. Hennion, H. Casalta, H. Andres, H.U. Güdel, A.V. Irodova, A. Caneschi, Phys. Rev. Lett. **83**, 628–631 (1999). https://doi.org/10.1103/PhysRevLett.83.628
37. S. Hill, Polyhedron **64**, 128–135 (2013). https://doi.org/10.1016/j.poly.2013.03.005

38. A. Chiesa, T. Guidi, S. Carretta, S. Ansbro, G.A. Timco, I. Vitorica-Yrezabal, E. Garlatti, G. Amoretti, R.E.P. Winpenny, P. Santini, Phys. Rev. Lett. **119**, 217202 (2017). https://doi.org/10.1103/PhysRevLett.119.217202

39. C. Delfs, D. Gatteschi, L. Pardi, R. Sessoli, K. Wieghardt, D. Hanke, Inorg. Chem. **32**, 3099–3103 (1993). https://doi.org/10.1021/ic00066a022

40. R. Caciuffo, G. Amoretti, A. Murani, R. Sessoli, A. Caneschi, D. Gatteschi, Phys. Rev. Lett. **81**, 4744–4747 (1998). https://doi.org/10.1103/PhysRevLett.81.4744

41. D. Gatteschi, R. Sessoli, A. Cornia, Chem. Commun. **1**, 725–732 (2000). https://doi.org/10.1039/A908254I

42. A. Cornia, M. Affronte, A.G.M. Jansen, D. Gatteschi, A. Caneschi, R. Sessoli, Chem. Phys. Lett. **322**, 477–482 (2000). https://doi.org/10.1016/S0009-2614(00)00464-4

43. A.L. Barra, P. Debrunner, D. Gatteschi, C.E. Schulz, R. Sessoli, Europhys. Lett. **35**, 133–138 (1996). https://doi.org/10.1209/epl/i1996-00544-3

44. G.A. Craig, M. Murrie, Chem. Soc. Rev. **44**, 2135–2147 (2015). https://doi.org/10.1039/C4CS00439F

45. J.M. Frost, K.L.M. Harriman, M. Murugesu, Chem. Sci. **7**, 2470–2491 (2016). https://doi.org/10.1039/C5SC03224E

46. D.E. Freedman, W.H. Harman, T.D. Harris, G.J. Long, C.J. Chang, J.R. Long, J. Am. Chem. Soc. **132**, 1224–1225 (2010). https://doi.org/10.1021/ja909560d

47. W.H. Harman, T.D. Harris, D.E. Freedman, H. Fong, A. Chang, J.D. Rinehart, A. Ozarowski, M.T. Sougrati, F. Grandjean, G.J. Long, J.R. Long, C.J. Chang, J. Am. Chem. Soc. **132**, 18115–18126 (2010). https://doi.org/10.1021/ja105291x

48. S. Mossin, B.L. Tran, D. Adhikari, M. Pink, F.W. Heinemann, J. Sutter, R.K. Szilagyi, K. Meyer, D.J. Mindiola, J. Am. Chem. Soc. **134**, 13651–13661 (2012). https://doi.org/10.1021/ja302660k

49. J.M. Zadrozny, D.J. Xiao, M. Atanasov, G.J. Long, F. Grandjean, F. Neese, J.R. Long, Nat. Chem. **5**, 577–581 (2013). https://doi.org/10.1038/nchem.1630

50. P.P. Samuel, K.C. Mondal, N. Amin, H.W. Roesky, E. Carl, R. Neufeld, D. Stalke, S. Demeshko, F. Meyer, L. Ungur, L.F. Chibotaru, J. Christian, V. Ramachandran, J. van Tol, N.S. Dalal, J. Am. Chem. Soc. **136**, 11964–11971 (2014). https://doi.org/10.1021/ja5043116

51. C.G. Werncke, M.-A. Bouammali, J. Baumard, N. Suaud, C. Martins, N. Guihéry, L. Vendier, J. Zheng, J.-B. Sortais, C. Darcel, S. Sabo-Etienne, J.-P. Sutter, S. Bontemps, C. Pichon, Inorg. Chem. **55**, 10968–10977 (2016). https://doi.org/10.1021/acs.inorgchem.6b01512

52. X. Feng, S.J. Hwang, J.-L. Liu, Y.-C. Chen, M.-L. Tong, D.G. Nocera, J. Am. Chem. Soc. **139**, 16474–16477 (2017). https://doi.org/10.1021/jacs.7b09699

53. J. Xiang, J.-J. Liu, X.-X. Chen, L.-H. Jia, F. Yu, B.-W. Wang, S. Gao, T.-C. Lau, Chem. Commun. **53**, 1474–1477 (2017). https://doi.org/10.1039/C6CC09801K

54. U. Chakraborty, S. Demeshko, F. Meyer, C. Rebreyend, B. de Bruin, M. Atanasov, F. Neese, B. Mühldorf, R. Wolf, Angew. Chem. Int. Ed. **56**, 7995–7999 (2017). https://doi.org/10.1002/anie.201702454

55. C.G. Werncke, L. Vendier, S. Sabo-Etienne, J.-P. Sutter, C. Pichon, S. Bontemps, Eur. J. Inorg. Chem. **1**, 1041–1406 (2017). https://doi.org/10.1002/ejic.201601461

56. M. Ding, A.K. Hickey, M. Pink, J. Telser, D.L. Tierney, M. Amoza, M. Rouzières, T.J. Ozumerzifon, W.A. Hoffert, M.P. Shores, E. Ruiz, R. Clérac, J.M. Smith, Chem. Eur. J. **25**, 10625–10632 (2019). https://doi.org/10.1002/chem.201900799

57. Y.-F. Deng, T. Han, Z. Wang, Z. Ouyang, B. Yin, Z. Zheng, J. Krzystek, Y.-Z. Zheng, Chem. Commun. **51**, 17688–17691 (2015). https://doi.org/10.1039/C5CC07025B

58. J. Vallejo, A. Pascual-Álvarez, J. Cano, I. Castro, M. Julve, F. Lloret, J. Krzystek, G. De Munno, D. Armentano, W. Wernsdorfer, R. Ruiz-García, E. Pardo, Angew. Chem. Int. Ed. **52**, 14075–14079 (2013). https://doi.org/10.1002/anie.201308047

59. A. Pascual-Álvarez, J. Vallejo, E. Pardo, M. Julve, F. Lloret, J. Krzystek, D. Armentano, W. Wernsdorfer, J. Cano, Chem. Eur. J. **21**, 17299–17307 (2015). https://doi.org/10.1002/chem.201502637

60. L. Chen, J. Wang, J.-Z. Liu, Y. Song, X.-T. Chen, Y.-Q. Zhang, Z.-L. Xue, Eur. J. Inorg. Chem. **1**, 271–278 (2015). https://doi.org/10.1002/ejic.201402964

61. J.M. Zadrozny, J. Liu, N.A. Piro, C.J. Chang, S. Hill, J.R. Long, Chem. Commun. **48**, 3927–3929 (2012). https://doi.org/10.1039/C2CC16430B

62. J.M. Zadrozny, J. Telser, J.R. Long, Polyhedron **64**, 209–217 (2013). https://doi.org/10.1016/j.poly.2013.04.008

63. L. Chen, J. Wang, J.-M. Wei, W. Wernsdorfer, X.-T. Chen, Y.-Q. Zhang, Y. Song, Z.-L. Xue, J. Am. Chem. Soc. **136**, 12213–12216 (2014). https://doi.org/10.1021/ja5051605

64. D. Schweinfurth, J. Krzystek, M. Atanasov, J. Klein, S. Hohloch, J. Telser, S. Demeshko, F. Meyer, F. Neese, B. Sarkar, Inorg. Chem. **56**, 5253–5265 (2017). https://doi.org/10.1021/acs.inorgchem.7b00371

65. H.-H. Cui, F. Lu, X.-T. Chen, Y.-Q. Zhang, W. Tong, Z.-L. Xue, Inorg. Chem. **58**, 12555–12564 (2019). https://doi.org/10.1021/acs.inorgchem.9b01175

66. J. Vallejo, M. Viciano-Chumillas, F. Lloret, M. Julve, I. Castro, J. Krzystek, M. Ozerov, D. Armentano, G. De Munno, J. Cano, Inorg. Chem. **58**, 15726–15740 (2019). https://doi.org/10.1021/acs.inorgchem.9b01719

67. K.E.R. Marriott, L. Bhaskaran, C. Wilson, M. Medarde, S.T. Ochsenbein, S. Hill, M. Murrie, Chem. Sci. **6**, 6823–6828 (2015). https://doi.org/10.1039/C5SC02854J

68. G.A. Craig, A. Sarkar, C.H. Woodall, M.A. Hay, K.E.R. Marriott, K.V. Kamenev, S.A. Moggach, E.K. Brechin, S. Parsons, G. Rajaraman, M. Murrie, Chem. Sci. **9**, 1551–1559 (2018). https://doi.org/10.1039/C7SC04460G

69. H.-H. Cui, W. Lv, W. Tong, X.-T. Chen, Z.-L. Xue, Eur. J. Inorg. Chem. **1**, 4653–4659 (2019). https://doi.org/10.1002/ejic.201900942

70. L. Wang, M. Zlatar, F. Vlahović, S. Demeshko, C. Philouze, F. Molton, M. Gennari, F. Meyer, C. Duboc, M. Gruden, Chem. Eur. J. **24**, 5091–5094 (2018). https://doi.org/10.1002/chem.201705989

71. J. Krzystek, J. Telser, Dalton Trans. **45**, 16751–16763 (2016). https://doi.org/10.1039/C6DT01754A

72. A.D. Adler, F.R. Longo, F. Kampas, J. Kim, J. Inorg. Nucl. Chem. **32**, 2443–2445 (1970). https://doi.org/10.1016/0022-1902(70)80535-8

73. A.K. Hassan, L.A. Pardi, J. Krzystek, A. Sienkiewicz, P. Goy, M. Rohrer, L.C. Brunel, J. Magn. Reson. **142**, 300–312 (2000). https://doi.org/10.1006/jmre.1999.1952

74. S.A. Zvyagin, J. Krzystek, P.H.M. van Loosdrecht, G. Dhalenne, A. Revcolevschi, Phys. B **346–347**, 1–5 (2004). https://doi.org/10.1016/j.physb.2004.01.009

75. J. Telser, eMagRes **6**, 207–234 (2017). https://doi.org/10.1002/9780470034590.emrstm1501

76. G. Aromí, J. Telser, A. Ozarowski, L.-C. Brunel, H.-M. Stoeckli-Evans, J. Krzystek, Inorg. Chem. **44**, 187–196 (2005). https://doi.org/10.1021/ic049180u

77. D.G. McGavin, W.C. Tennant, J.A. Weil, J. Magn. Reson. **87**, 92–109 (1990). https://doi.org/10.1016/0022-2364(90)90088-Q

78. J. Krzystek, S.A. Zvyagin, A. Ozarowski, S. Trofimenko, J. Telser, J. Magn. Reson. **178**, 174–183 (2006). https://doi.org/10.1016/j.jmr.2005.09.007

79. K. Ray, A. Begum, T. Weyhermüller, S. Piligkos, J. van Slageren, F. Neese, K. Wieghardt, J. Am. Chem. Soc. **127**, 4403–4415 (2005). https://doi.org/10.1021/ja042803i

80. S.-D. Jiang, D. Maganas, N. Levesanos, E. Ferentinos, S. Haas, K. Thirunavukkuarasu, J. Krzystek, M. Dressel, L. Bogani, F. Neese, P. Kyritsis, J. Am. Chem. Soc. **137**, 12923–12928 (2015). https://doi.org/10.1021/jacs.5b06716

81. Y. Rechkemmer, J.E. Fischer, R. Marx, M. Dörfel, P. Neugebauer, S. Horvath, M. Gysler, T. Brock-Nannestad, W. Frey, M.F. Reid, J. van Slageren, J. Am. Chem. Soc. **137**, 13114–13120 (2015). https://doi.org/10.1021/jacs.5b08344

82. Y. Rechkemmer, F.D. Breitgoff, M. van der Meer, M. Atanasov, M. Hakl, M. Orlita, P. Neugebauer, F. Neese, B. Sarkar, J. van Slageren, Nat. Commun. **7**, 10467 (2016). https://doi.org/10.1038/ncomms10467

83. D.H. Moseley, S.E. Stavretis, Z. Zhu, M. Guo, C.M. Brown, M. Ozerov, Y. Cheng, L.L. Daemen, R. Richardson, G. Knight, K. Thirunavukkuarasu, A.J. Ramirez-Cuesta, J. Tang, Z.-L. Xue, Inorg. Chem. **59**, 5218–5230 (2020). https://doi.org/10.1021/acs.inorgchem.0c00523

84. S.E. Stavretis, D.H. Moseley, F. Fei, H.-H. Cui, Y. Cheng, A.A. Podlesnyak, X. Wang, L.L. Daemen, C.M. Hoffmann, M. Ozerov, Z. Lu, K. Thirunavukkuarasu, D. Smirnov, T. Chang, Y.-S. Chen, A.J. Ramirez-Cuesta, X.-T. Chen, Z.-L. Xue, Chem. Eur. J. **25**, 15846–15857 (2019). https://doi.org/10.1002/chem.201903635

85. D.H. Moseley, S.E. Stavretis, K. Thirunavukkuarasu, M. Ozerov, Y. Cheng, L.L. Daemen, J. Ludwig, Z. Lu, D. Smirnov, C.M. Brown, A. Pandey, A.J. Ramirez-Cuesta, A.C. Lamb, M. Atanasov, E. Bill, F. Neese, Z.-L. Xue, Nat. Commun. **9**, 2572 (2018). https://doi.org/10.1038/s41467-018-04896-0

86. C.N. Widener, A.N. Bone, M. Ozerov, R. Richardson, Z. Lu, K. Thirunavukkuarasu, D. Smirnov, X.-T. Chen, Z.-L. Xue, Chin. J. Inorg. Chem. **35**, 1149–1156 (2020). https://doi.org/10.11862/CJIC.2020.126

87. S. Stoll, A. Schweiger, J. Magn. Reson. **178**, 42–55 (2006). https://doi.org/10.1016/j.jmr.2005.08.013

88. J. Nehrkorn, K. Holldack, R. Bittl, A. Schnegg, J. Magn. Reson. **280**, 10–19 (2017). https://doi.org/10.1016/j.jmr.2017.04.001

89. J. Lu, I.O. Ozel, C.A. Belvin, X. Li, G. Skorupskii, L. Sun, B.K. Ofori-Okai, M. Dincă, N. Gedik, K.A. Nelson, Chem. Sci. **8**, 7312–7323 (2017). https://doi.org/10.1039/C7SC00830A

90. G.C. Brackett, Ph.D. Dissertation, University of California, 1970. https://escholarship.org/content/qt2s50c1gm/qt2s50c1gm.pdf

91. A. Furrer, J. Mesot, T. Strässle, *Neutron Scattering in Condensed Matter Physics* (World Scientific, Singapore, 2009)

92. A. Furrer, O. Waldmann, Rev. Mod. Phys. **85**, 367–420 (2013). https://doi.org/10.1103/RevModPhys.85.367

93. J.J. Borrás-Almenar, J.M. Clemente-Juan, E. Coronado, B.S. Tsukerblat, Inorg. Chem. **38**, 6081–6088 (1999). https://doi.org/10.1021/ic990915i

94. M.A. Dunstan, R.A. Mole, C. Boskovic, Eur. J. Inorg. Chem. **1**, 1090–1105 (2019). https://doi.org/10.1002/ejic.201801306

95. Z.-L. Xue, A.J. Ramirez-Cuesta, C.M. Brown, S. Calder, H. Cao, B.C. Chakoumakos, L.L. Daemen, A. Huq, A.I. Kolesnikov, E. Mamontov, A.A. Podlesnyak, X. Wang, Eur. J. Inorg. Chem. **1**, 1065–1089 (2019). https://doi.org/10.1002/ejic.201801076

96. H. Andres, R. Basler, H.-U. Güdel, G. Aromí, G. Christou, H. Büttner, B. Rufflé, J. Am. Chem. Soc. **122**, 12469–12477 (2000). https://doi.org/10.1021/ja0009424

97. G. Carver, P.L.W. Tregenna-Piggott, A.-L. Barra, A. Neels, J.A. Stride, Inorg. Chem. **42**, 5771–5777 (2003). https://doi.org/10.1021/ic034110t

98. R. Basler, A. Sieber, G. Chaboussant, H.U. Güdel, N.E. Chakov, M. Soler, G. Christou, A. Desmedt, R. Lechner, Inorg. Chem. **44**, 649–653 (2005). https://doi.org/10.1021/ic048931p

99. K.R. Kittilstved, L.A. Sorgho, N. Amstutz, P.L.W. Tregenna-Piggott, A. Hauser, Inorg. Chem. **48**, 7750–7764 (2009). https://doi.org/10.1021/ic900613p

100. J. Dreiser, O. Waldmann, C. Dobe, G. Carver, S.T. Ochsenbein, A. Sieber, H.U. Güdel, J. van Duijn, J. Taylor, A. Podlesnyak, Phys. Rev. B **81**, 024408 (2010). https://doi.org/10.1103/PhysRevB.81.024408

101. C.H. Wang, M.D. Lumsden, R.S. Fishman, G. Ehlers, T. Hong, W. Tian, H. Cao, A. Podlesnyak, C. Dunmars, J.A. Schlueter, J.L. Manson, A.D. Christianson, Phys. Rev. B **86**, 064439 (2012). https://doi.org/10.1103/PhysRevB.86.064439

102. M.J. Giansiracusa, M. Vonci, W. Van den Heuvel, R.W. Gable, B. Moubaraki, K.S. Murray, D. Yu, R.A. Mole, A. Soncini, C. Boskovic, Inorg. Chem. **55**, 5201–5214 (2016). https://doi.org/10.1021/acs.inorgchem.6b00108

103. L. Chen, H.-H. Cui, S.E. Stavretis, S.C. Hunter, Y.-Q. Zhang, X.-T. Chen, Y.-C. Sun, Z. Wang, Y. Song, A.A. Podlesnyak, Z.-W. Ouyang, Z.-L. Xue, Inorg. Chem. **55**, 12603–12617 (2016). https://doi.org/10.1021/acs.inorgchem.6b01544

104. S.E. Stavretis, Y. Cheng, L.L. Daemen, C.M. Brown, D.H. Moseley, E. Bill, M. Atanasov, A.J. Ramirez-Cuesta, F. Neese, Z.-L. Xue, Eur. J. Inorg. Chem. **1**, 1119–1127 (2019). https://doi.org/10.1002/ejic.201801088

105. A.N. Bone, S.E. Stavretis, J. Krzystek, Z. Liu, Q. Chen, Z. Gai, X. Wang, C.A. Steren, X.B. Powers, A.A. Podlesnyak, X.-T. Chen, J. Telser, H. Zhou, Z.-L. Xue, Polyhedron **184**, 114488 (2020). https://doi.org/10.1016/j.poly.2020.114488

106. E. Colacio, J. Ruiz, E. Ruiz, E. Cremades, J. Krzystek, S. Carretta, J. Cano, T. Guidi, W. Wernsdorfer, E.K. Brechin, Angew. Chem. Int. Ed. **52**, 9130–9134 (2013). https://doi.org/10.1002/anie.201304386

107. J. Dreiser, A. Schnegg, K. Holldack, K.S. Pedersen, M. Schau-Magnussen, J. Nehrkorn, P. Tregenna-Piggott, H. Mutka, H. Weihe, J. Bendix, O. Waldmann, Chem. Eur. J. **17**, 7492–7498 (2011). https://doi.org/10.1002/chem.201100581

108. D. Pinkowicz, H.I. Southerland, C. Avendaño, A. Prosvirin, C. Sanders, W. Wernsdorfer, K.S. Pedersen, J. Dreiser, R. Clérac, J. Nehrkorn, G.G. Simeoni, A. Schnegg, K. Holldack, K.R. Dunbar, J. Am. Chem. Soc. **137**, 14406–14422 (2015). https://doi.org/10.1021/jacs.5b09378

109. R. Basler, P.L.W. Tregenna-Piggott, H. Andres, C. Dobe, H.-U. Güdel, S. Janssen, G.J. McIntyre, J. Am. Chem. Soc. **123**, 3377–3378 (2001). https://doi.org/10.1021/ja003801a

110. A. Sieber, C. Boskovic, R. Bircher, O. Waldmann, S.T. Ochsenbein, G. Chaboussant, H.U. Güdel, N. Kirchner, J. van Slageren, W. Wernsdorfer, A. Neels, H. Stoeckli-Evans, S. Janssen, F. Juranyi, H. Mutka, Inorg. Chem. **44**, 4315–4325 (2005). https://doi.org/10.1021/ic050134j

111. M. Sigrist, P.L.W. Tregenna-Piggott, K.S. Pedersen, M.A. Sørensen, A.-L. Barra, J. Hauser, S.-X. Liu, S. Decurtins, H. Mutka, J. Bendix, Eur. J. Inorg. Chem. **1**, 2683–2689 (2015). https://doi.org/10.1002/ejic.201500084

112. R. Bircher, G. Chaboussant, S.T. Ochsenbein, F. Fernandez-Alonso, H.U. Güdel, E.K. Brechin, Polyhedron **24**, 2455–2458 (2005). https://doi.org/10.1016/j.poly.2005.03.062

113. S. Ansbro, E. Moreno-Pineda, W. Yu, J. Ollivier, H. Mutka, M. Ruben, A. Chiesa, Dalton Trans. **47**, 11953–11959 (2018). https://doi.org/10.1039/C8DT02570C

114. M.L. Baker, T. Guidi, S. Carretta, J. Ollivier, H. Mutka, H.U. Güdel, G.A. Timco, E.J.L. McInnes, G. Amoretti, R.E.P. Winpenny, P. Santini, Nat. Phys. **8**, 906–911 (2012). https://doi.org/10.1038/nphys2431

115. E. Garlatti, T. Guidi, S. Ansbro, P. Santini, G. Amoretti, J. Ollivier, H. Mutka, G. Timco, I.J. Vitorica-Yrezabal, G.F.S. Whitehead, R.E.P. Winpenny, S. Carretta, Nat. Commun. **8**, 14543 (2017). https://doi.org/10.1038/ncomms14543

116. E. Garlatti, A. Chiesa, T. Guidi, G. Amoretti, P. Santini, S. Carretta, Eur. J. Inorg. Chem. **1**, 1106–1118 (2019). https://doi.org/10.1002/ejic.201801050

117. S. Gómez-Coca, A. Urtizberea, E. Cremades, P.J. Alonso, A. Camón, E. Ruiz, F. Luis, Nat. Commun. **5**, 4300 (2014). https://doi.org/10.1038/ncomms5300

118. G.J. Long, *Mössbauer Spectroscopy Applied to Inorganic Chemistry* (Springer, Heidelberg, 1984)

119. D. Gatteschi, L. Sorace, J. Solid State Chem. **159**, 253–261 (2001). https://doi.org/10.1006/jssc.2001.9154

120. J. Krzystek, A. Ozarowski, J. Telser, Coord. Chem. Rev. **250**, 2308–2324 (2006). https://doi.org/10.1016/j.ccr.2006.03.016

121. D. Gatteschi, L. Sorace, R. Sessoli, A.L. Barra, Appl. Magn. Reson. **21**, 299–310 (2001). https://doi.org/10.1007/BF03162409

122. S. Mossin, H. Weihe, A.-L. Barra, J. Am. Chem. Soc. **124**, 8764–8765 (2002). https://doi.org/10.1021/ja012574p

123. S. Shova, A. Vlad, M. Cazacu, J. Krzystek, L. Bucinsky, M. Breza, D. Darvasiová, P. Rapta, J. Cano, J. Telser, V.B. Arion, Dalton Trans. **46**, 11817–11829 and references therein by C. Duboc and coworkers (2017). https://doi.org/10.1039/C7DT01809F.

124. J. Krzystek, J. Telser, L.A. Pardi, D.P. Goldberg, B.M. Hoffman, L.-C. Brunel, Inorg. Chem. **38**, 6121–6129 (1999). https://doi.org/10.1021/ic9901970

125. D.S. McClure, Solid State Phys. **9**, 399–525 (1959). https://doi.org/10.1016/S0081-1947(08)60569-X

126. NIST, NIST Atomic Spectra Database Levels Form (https://physics.nist.gov/PhysRefData/ASD/levels_form.html).

Publisher's Note Springer Nature remains neutral with regard to jurisdictional claims in published maps and institutional affiliations.

Affiliations

Pagnareach Tin[1] · Shelby E. Stavretis[1] · Mykhaylo Ozerov[2] · J. Krzystek[2] · A. N. Ponomaryov[3,7] · S. A. Zvyagin[3] · J. Wosnitza[3,4] · Ching-Chin Chen[5] · Peter P.-Y. Chen[5] · Joshua Telser[6] · Zi-Ling Xue[1]

✉ J. Krzystek
  krzystek@magnet.fsu.edu

✉ Zi-Ling Xue
    xue@utk.edu

1   Department of Chemistry, University of Tennessee, Knoxville, TN 37996, USA

2   National High Magnetic Field Laboratory, Florida State University, Tallahassee, FL 32310,
    USA

3   Dresden High Magnetic Field Laboratory (HLD-EMFL) and Würzburg-Dresden Cluster
    of Excellence ct.qmat, Helmholtz-Zentrum Dresden-Rossendorf, 01328 Dresden, Germany

4   Institut für Festkörper- und Materialphysik, Technische Universität Dresden, 01062 Dresden,
    Germany

5   Department of Chemistry, National Chung Hsing University, Taichung 402, Taiwan

6   Department of Biological, Physical and Health Sciences, Roosevelt University, Chicago,
    IL 60605, USA

7   Present Address: Institute of Radiation Physics, Helmholtz-Zentrum Dresden-Rossendorf,
    01328 Dresden, Germany